Title Page

The name(s) of the author(s)

(1) Aniruddha Bhattacharya (Corresponding Author)

(2) Madhusudan Singh

A concise and informative title:

"Performance analysis of TCT Smart controllers for islanded Microgrid"

The affiliation(s) and address(es) of the author(s:

(1) **Department of Electrical Engineering Delhi Technological University Bawana Road Delhi; 110042**

(2) **Department of Electrical Engineering Delhi Technological University Bawana Road Delhi; 110042**

RUNNING TITLE: **"Performance analysis of Tripatriate Smart controllers for islanded Microgrid"**

The e-mail address, telephone and fax numbers of the corresponding author

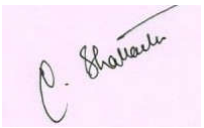

ANIRUDDHA BHATTACHARYA (CORRESPONDING AUTHOR)

Performance analysis of Tripartite Smart controllers for islanded Micro grid

***Aniruddha Bhattacharya , Madhusudan Singh,**

Abstract: This paper presents implementation of control method for dual control of VIC (Voltage and Current control) and Power sharing coupled with Demand Response for the islanded microgrid. These three controller viz VI controller (VIC), Power sharing controller(PSC) and smart load controller(SLC) while acting in unison can able to maintain long layoff from the connection requirement of the main grid. The paper uses state space inverter based generator model with close loop VIC and PSC will enhance microgrid stability and transient response where smart load controller which uses state space model for voltage ,current and PLL units to estimate reserve power available from smart load for better voltage and frequency regulation. VIC-PSC will also assist the microgrid for smooth disconnection of microgrid from main grid while SLC will use its point of load voltage control for smooth islanding of microgrid. This control technique henceforth called tripartite control technique (TCT), compared with classical controller connected to microgrid in maintaining frequency, voltage with power sharing of the inverter driven by renewable generator. This paper investigate the operation performance issues of test Microgrid with TCT. Simulation results indicate close approximation with experimental results

Keywords: Tripartite Control Technique (TCT), VI controller, SLC controller, Power Sharing controller (PSC), VIC-PSC, Distributed Energy Resources (DER)

1 Introduction: The U.S. Department of Energy (DOE) defines a microgrid as "*a group of interconnected loads and distributed energy resources within clearly defined electrical boundaries that acts as a single controllable entity with respect to the grid. A microgrid can connect and disconnect from the grid to enable it to operate in both grid-connected or island-mode".* The major challenges of microgrid faces during islanding is lack of standard voltage , frequency and phase contrary to grid connection where inertial factor do come to the rescue of control scheme meant for achieving power quality. The proportion of power electronic devices is expected to increase in future like inverter interfaced distributed generators (DGs). It will present significant challenge in maintaining power quality in the microgrid. VI control as primary control with highest bandwidth followed by PSC/PQ(DER Power Sharing control) as secondary control may be enough to maintain power quality barring severe contingences like sudden DER loss where tertiary control of demand response with point of Load voltage control with SLC[8] . Thus it produces additional power reserve for droop control mechanism and power tracking for frequency and phase restoration With more non-

linear capacitive loads getting connected to distribution network this situation will going to worse, as shown in [1][3], where impedance measurements were carried out in the residential distribution network. Resonance at low frequencies will result in rise in harmonic voltages which may lead to unstable operation of DG inverters. Stability analysis of distribution networks with inverter connected DGs is an active area of research. It is important to study the control loop dynamics of the different inverters and their interaction with other power electronic devices connected to the network. In [2], a transfer function based stability analysis has been proposed to characterize the dynamics of the interconnected feedback loops in the system. Different case studies have been formulated to evaluate distribution network stability when subjected to frequency, load and power set-point disturbances. In [2], stability analysis has been carried out for a microgrid having active loads connected in parallel to DG inverters. Through linearised state space analysis, it has been shown that active loads (constant power behavior) having control loop dynamics in a similar frequency range to the DG inverters may lead to degradation of the damping of the network. Further, through participation analysis of system eigenvalues, it was identified that the low frequency modes are associated with the DG inverter droop control and the voltage controller of the active loads. Similar studies have also been presented in [3].The operation of multiple active load for the purpose of voltage and/or frequency regulation has been studied previously. However, in the majority of these studies [4], [5], [6], the active load along with the noncritical loads are represented as controllable current or power sources. Vector control of DG inverters and active loads is commonly used for Stability studies. To make use of the standard analysis techniques already existing, it is important to develop vector control of active loads which will make it easier to integrate into the stability model of the distribution network with other power electronic devices. An overview of the various control schemes proposed so far in the literature for SLQ and SLBC type smart loads is presented in [8][9][10]. While vector control of SLBC is very similar to DVR control and has already been proposed in [22], dq control scheme for SLQ is more challenging and is the focus of this paper. The dynamic modelling of SLQ has previously been presented in [23].However, the control scheme is not based on dq framework. Hence, the tuning of the controller gains, unlike vector control, are not based on analytical methods. Moreover, it lacks a inner current control loop which is necessary for limiting the inverter current within safe limits. Further, a state-space model of SLQ is reported in [23] based on the dynamic model in [24]. However, it is not compatible with the standard modelling framework for power quality analysis and does not analyse the impact of change in distribution network parameters and power references for tracking due to sudden loss of DER[15][16][17] The absence of vector control and a linearized state space model for

reliability analysis through three stage hierarchical (primary , secondary and tertiary) control has motivated the work. Furthermore due to the fundamental difference in principle of operation of synchronous generators (SGs) and power electronic interfaced NSGs(non synchronous generator), the contribution to system strength in terms of short circuit level depends on the technology employed and is, in general, lower than SGs[17][18][19]. This can lead to wider voltage variations during a disturbance and threaten system reliability. To support system inertia and stabilize grid frequency and nodal voltages in case of a large disturbance, collective participation of loads (demand response) will increasingly play an important role in maintaining the reliability of the microgrid[20[21]

2. Novel open-loop state-space model of an inverter-based generator that includes V-I and power sharing dynamics with demand response control

The proposed model for this research is obtained in two stages. First, the model of each inverter connected to the main grid is used to describe dynamics in grid-connected mode. This model is also used to develop the proposed control strategy. Then, the models of all inverters are integrated in a single state-space model to describe microgrid dynamics in islanded mode[3][4]. The islanded microgrid model was used to assess stability and robustness of the proposed controller in islanded mode. For grid-connected mode, the state-space model must be used for each generator individually[5][6]. The circuit considered for the islanded microgrid model is shown in Fig. 1. Although, many types of loads may exist in microgrids, the load is selected to be an smart load which uses point of Load voltage control which permits controlling the power consumption of an aggregate load (which exhibits certain voltage dependency) instead of using just thermostatic loads for Demand response (DR) because it is the most common type of load found in residential and industrial environments. It can provide independent control of active and reactive compensation which allows it to Operate in all the four quadrants. Distributed control of voltage using Point of Load (PoL) Voltage regulator does not rely on communication infrastructure and is able to take decisions (amount of DR to be exercised) based on local measurements. *d-q* state models of the Load may also be obtained and integrated with the microgrid model for performance evaluation of islanded microgrid.

***3. d-q* model of microgrid**

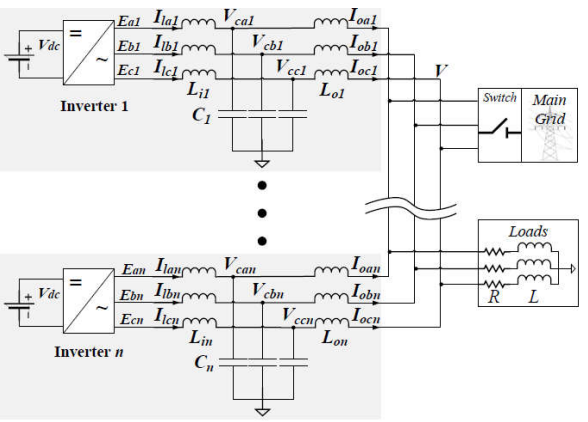

Fig 1 Complete islanded microgrid scheme with an voltage controlled Load (PoL type)

To obtain the complete microgrid- Load model in islanded mode, the model for one phase of each inverter using (2) must be computed. Then, V must be defined in terms of the output currents and load components as follows:

$$V = L\frac{dIot}{dt} + R\ Iot \qquad (1)$$

where $Iot = \Sigma\ Ioj\ nj{=}1$ with n representing the number of generators. A complete microgrid model is obtained by substituting V from (1) into the model of each inverter and combining two models of generators with a smart PoL voltage controlled load, the microgrid model in islanded mode for one phase is given by (2).

$$\begin{pmatrix} Vc1 \\ It1 \\ Ic1 \\ Vc2 \\ It2 \\ Ic2 \end{pmatrix} = \begin{pmatrix} 0 & \frac{1}{C1} & -\frac{1}{C1} & 0 & 0 & 0 \\ -\frac{1}{Li1} & 0 & 0 & 0 & 0 & 0 \\ \frac{Lt2}{Lt} & 0 & RL-\frac{RLt2}{Lt} & -\frac{L}{Lt} & 0 & -\frac{1}{C2} \\ 0 & 0 & 0 & 0 & \frac{1}{C2} & -\frac{1}{C2} \\ 0 & 0 & 0 & -\frac{1}{Lt2} & 0 & 0 \\ -\frac{L}{Lt} & 0 & RL-\frac{RLt1}{Lt} & \frac{Lt1}{Lt} & 0 & \frac{RL-RLt1}{Lt} \end{pmatrix} \begin{pmatrix} Vc1 \\ It1 \\ Io1 \\ Vc2 \\ It2 \\ Io2 \end{pmatrix} + \begin{bmatrix} 0 & 0 \\ \frac{1}{Lt1} & 0 \\ 0 & 0 \\ 0 & 0 \\ 0 & \frac{1}{Lt2} \\ 0 & 0 \end{bmatrix} \begin{bmatrix} E1 \\ E2 \end{bmatrix}$$

(2)

where $L_t{=}L(L_{o1}{+}L_{o2}){+}L_{o1}L_{o2}$, $Lt1{=}L{+}L_{o1}$, and $L_{t2}{=}L{+}L_{o2}$. For two inverters, replacing V from (1) into each generator model yields to a linear system with the differential equations for the output currents as shown in (2). Combining the solution of each of the model of each inverter, the complete microgrid model (2) for n inverters may be obtained. The model in (2) is for each phase. However, it must be transformed to the dq frame using (3).

The state-space model (3) is obtained using the dq transformation [3]. The dq transformation is performed by assuming a constant angular frequency ωc, which corresponds to the nominal angular frequency of the main grid.

$$\dot{x} = Adq + \mathrm{B_{1dq}}\ \mathrm{E_{dq}} + \mathrm{B_{2dq}}\ \mathrm{V_{dq}} \qquad (3)$$

$$\mathrm{A_{dq}} = \begin{pmatrix} 0 & \omega c & 1/C & 0 & -1/C & 0 \\ -\omega c & 0 & 0 & 1/C & 0 & -1/C \\ -1/Lt & 0 & 0 & \omega c & 0 & 0 \\ 0 & -1/Lt & -\omega c & 0 & 0 & 0 \\ 1/Lo & o & 0 & 0 & 0 & \omega c \\ 0 & 1/Lo & 0 & 0 & -\omega c & 0 \end{pmatrix} \qquad (4)$$

$$\mathrm{X} = \begin{pmatrix} Vcd \\ Vcq \\ Ild \\ Ilq \\ Iod \\ Ioq \end{pmatrix} \quad \mathrm{B_{1dq}} = \begin{pmatrix} 0 & 0 \\ 0 & 0 \\ \frac{1}{Lt} & 0 \\ 0 & \frac{1}{Lt} \\ 0 & 0 \\ 0 & 0 \end{pmatrix} \quad \mathrm{E_{dq}} = \begin{pmatrix} Ed \\ Eq \end{pmatrix} \quad \mathrm{B_{2dq}} = \begin{pmatrix} 0 & 0 \\ 0 & 0 \\ 0 & 0 \\ 0 & 0 \\ -\frac{1}{Lo} & 0 \\ 0 & -1/Lo \end{pmatrix}$$

The dq frame is synchronized with Va by using a PLL so that $Vdq{=}[\bar{V}d0]T$, where $\bar{V}d$ represents the nominal voltage peak amplitude of the main grid[7]. Thus, the output of the state-space model is used to represent the active and reactive power received by Vdq as follows:

$$P = \frac{3}{2}(VdId + VqIq)$$

$$Q = \frac{3}{2}(VqId - VdIq) \qquad (5)$$

Formulating the model in the dq frame as in (3) allows computing the power injected from Edq to Vdq by applying the superposition principle[10]

4. Integrated PQVI Controller

The discrete-time TCT controller optimization problem defines a cost function that weighs the sum of squares of the system input E_{dq} $[k]$ and the output error e$[k]$ = y$[k]$ − r$[k]$. The discrete TCT controller cost function is given by [2], [3][4]:

$$J(K0) = \frac{1}{2}\sum_{k=K0}^{T}(eT[k]Q_p\ e[k] + E_{dq}{}^{T}[k]\ R_p\ E_{dq}[k])$$

(6)

Where Qp is a symmetric positive-semi-definite weighting matrix and Rp is a symmetric positive-definite weighting matrix. The control scheme of the TCT controller is shown in Fig. 2.

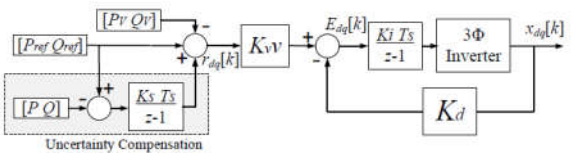

Fig No. 2 Control scheme for the TCT controller

The discrete-time state-space model of the three-phase inverter is given by[8][11][12]:

$$x_{dq}[k+1] = A\ dq\ xdq[k] + B1dq\ Edq[k]$$

$$y = C\ xdq\ [k]$$

$$Edq = -Kd\ xdq\ [k] + Kv\ v\ rdq\ [k]$$

$$Kd = \left(B_{1dq}^{T} S\ B_{1dq} + Rp\right)^{-1} B_{1dq}^{T} S\ A_{(dq)}$$

Where $\bar{A}$, $\bar{B}1dq$, and C are the discrete-time state, input, and output matrices in

the dq frame, respectively. The control law is given by:

$$E_{dq} = -K_d x_{dq}[k] + K_v v r_{dq}[k].$$

$$Kv = \left(B_{1dq}^{T} S\ B_{1dq} + Rp\right)^{-1} B_{1dq}^{T}$$

$$V_{[k+1]} = Adq - B1dqKd)^{T}\ \dot{v}[k] + C^{T}\ Qp\ r[k]$$

$$V_{[k+1]} = V_{[k}$$

$$\upsilon = [1 - (A_{dq} - B_{1dq}Kd)^{T}]^{-1}\ C^{T}\ Q_p$$

$$R(z) = \begin{pmatrix} Pref \\ Qref \end{pmatrix} - \begin{pmatrix} Pv \\ Qv \end{pmatrix} + \frac{KsTs}{z-1}\begin{pmatrix} Pref-P \\ Qref-Q \end{pmatrix}$$

Where (z)=Z$\{r[k]\}$, with Z$\{\cdot\}$ being the z-transform. Terms P and Q represent the measured power injected to the common bus in islanded mode. An integrator with a low-gain Ks is used to eliminate power tracking error induced by uncertainties in the AC bus or component values, without affecting stability margins. In addition, the AC bus power contribution vector $[P_V Q_V]$ is subtracted from the power reference vector $[PrefQref]$ to obtain the net power reference. To compute P_V and Q_V, the superposition principle must be used by solving the

following closed-loop state-space model with infinite horizon for r[k] =[0 0]T and Vdq=[$\bar{V}d$0]T

5.Proportional Power Sharing and Voltage Restoration model

Voltage restoration loop is used to recover voltage deviations when the microgrid is operating in islanded mode. A control scheme for the voltage restoration loop is shown in Fig. 3. When the main grid connection is lost, the voltage in the AC bus drops and the Grid Connection Flag becomes zero. The detection of grid disconnection is

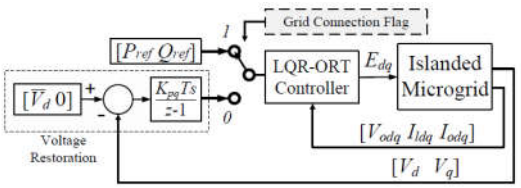

Fig 3: Voltage Restoration Loop Control

Assumed. Its development is out of the scope of this paper. To restore AC bus voltage without communications, a supplementary loop is implemented on each inverter. This loop integrates the error of Vdq referred to V^{-} . The output of this integrator becomes the new power reference of the TCT controller

$$Pref = Kpi\frac{Ts}{z-1}(Vd - \dot{Vd}) \quad (5)$$

$$Qref = \frac{KqiTs}{z-1}(Vq) \quad (6)$$

The active power gain Kpi must be positive and the reactive power gain Kqi must be negative. In steady state, $Prefi = Pi$ for the TCT controller. Then, for a pair of inverters connected to the AC bus.

$$P1/\ P2 = Kp1\ /Kp2 \quad (6\text{ -a})$$

$$Q1\ /\ Q2 = Kq1\ /Kq2.$$

6. Inverter Synchronization and Frequency Restoration model

To synchronize each inverter with the AC bus, a Second Order Integrator-Phase Locked Loop (SOI-PLL) is used as shown in Fig. 4 [5]. The output of the SOI-PLL is used to perform the *dq* transformation of the input and output signals for the TCT controller. When grid connection is lost, the operating frequency of the microgrid drops and the frequency restoration loop is activated. The frequency restoration loop integrates the frequency error and compensates the PLL operating frequency ω'. Hence, the output frequency of each generator will increase and the microgrid frequency returns to the nominal value in islanded mode. Thus, the proposed frequency restoration loop gives the capability of working in both grid-connected and islanded modes not only to the proposed TCT controller, but also to smart load controller implemented in the *dq* frame. The expression for the output frequency of the SOI-PLL with the frequency restoration

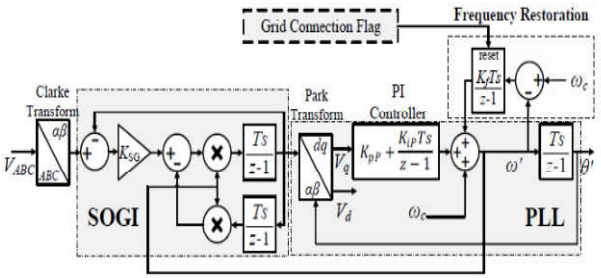

Fig No.4 **SOGI-PLL with frequency restoration loop**

$$\omega' = Vq\ \left(Kp\ P + KiP\frac{Ts}{z-1}\right) + \omega c + Fg\ Kf\frac{Ts}{z-1}(\omega' - \omega c)\ (7)$$

where Fg is one when grid connection is lost and $Fg = 0$ when the grid is engaged. Assuming that the SOI-PLL is synchronized, such that $Vq = 0$, it can be noted that in steady-state, $z \rightarrow 1$ and $\omega' \approx \omega_c$ as above in (7).

7. Complete TCT Control Scheme

The complete TCT control scheme for one inverter is shown in Fig.4. Each inverter has its own PLL-SOGI synchronized with the AC bus. The output of the PLL-SOGI is used to perform the *dq* conversion of the states and control input. When the microgrid is connected to the main grid, each inverter works as a grid-following generator. This means that the AC bus voltage and frequency are imposed by the main grid. When grid connection is lost, the Grid Connection Flag is activated, each inverter starts working as a grid-forming generator, and the voltage and frequency restoration loops are engaged. But this control will be augmented by smart load controller which will produce excess Power reserve - ΔP_{SL} during frequency droop by Point of Load voltage control of static load as shown in Fig 5 and explained in the later section in (8)

8. Complete Schematic of Microgrid with complete Control with constant impedance RL load

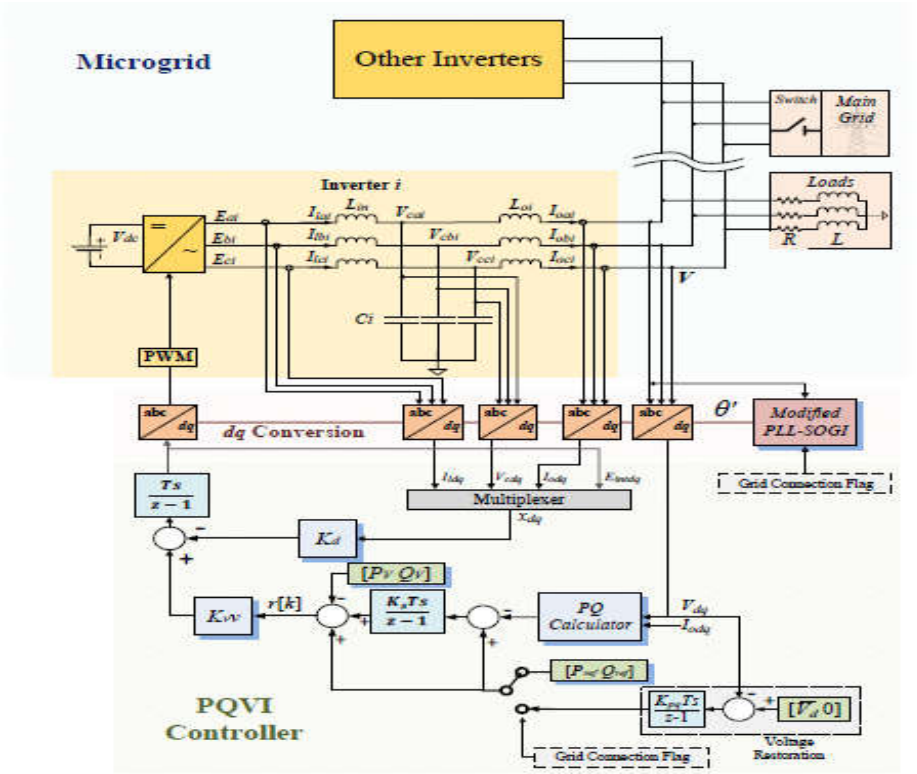

Fig No. 5 **Microgrid Model**

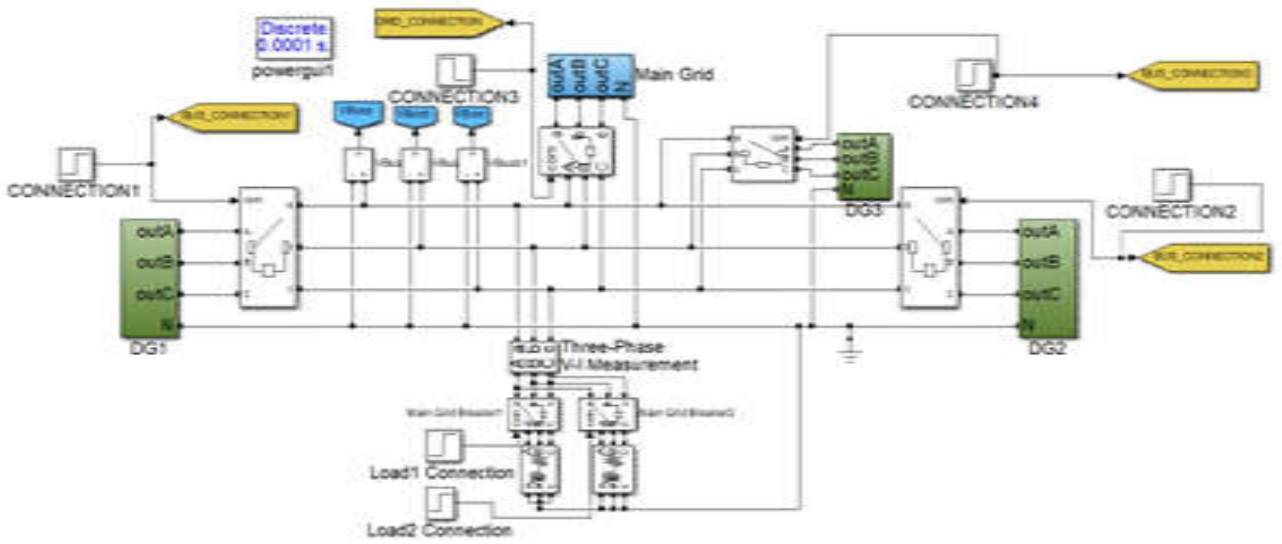

Fig No.6 Microgrid Simulink Model

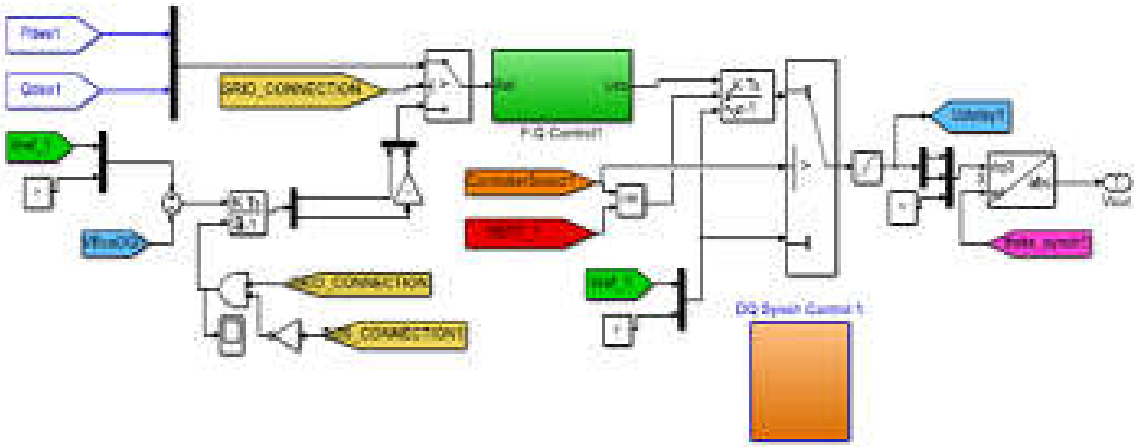

Fig No.7 Simulink Block Diagram for the Integrated PQVI Controller

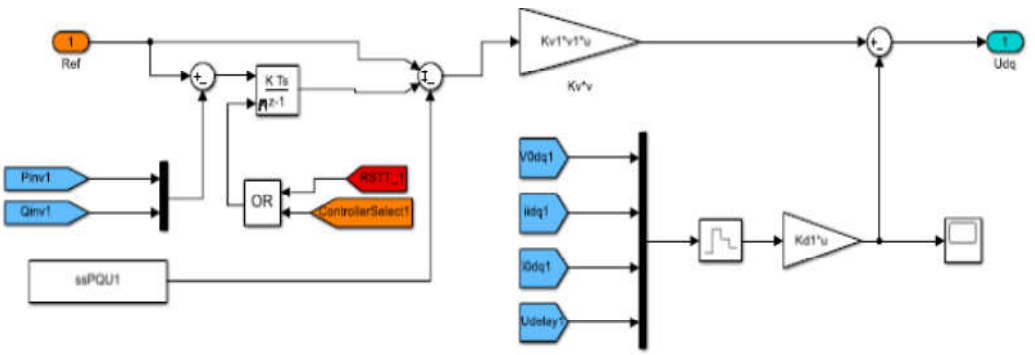

Fig No.8 Simulink Block Diagram for the TCT CONTROLLER

9. Numerical Values for the Proposed SIMULATIONS

State-space models of each inverter connected to the main grid and the entire microgrid in islanded mode are presented. Discrete state-space models are presented in the *dq* frame. Sampling frequency was defined to be fs=10 kHz according to Shannon sampling theory [6]. This selection allows controller regulating harmonics up to 17-th order equivalent to f_{h17}=1,020Hz. Computed controllers are only presented in discrete-time.

9.1 Islanded Microgrid:

$$\bar{A}_{dq1} =$$

$$\begin{bmatrix} 0.4321 & 0.0163 & 9.1123 & 0.3437 & -9.1123 & -0.3437 & 0.2837 & 0.0070 \\ -0.0163 & 0.4321 & -0.3437 & 9.1123 & 0.3437 & -9.1123 & -0.0070 & 0.2837 \\ -0.0445 & -0.0017 & 0.7157 & 0.0270 & 0.2836 & 0.0107 & 0.0501 & 0.0009 \\ 0.0017 & -0.0445 & -0.0270 & 0.7157 & -0.0107 & 0.2836 & -0.0009 & 0.0501 \\ 0.0445 & 0.0017 & 0.2836 & 0.0107 & 0.7157 & 0.0270 & 0.0055 & 0.0002 \\ -0.0017 & 0.0445 & -0.0107 & 0.2836 & -0.0270 & 0.7157 & -0.0002 & 0.0055 \\ 0 & 0 & 0 & 0 & 0 & 0 & 1 & 0 \\ 0 & 0 & 0 & 0 & 0 & 0 & 0 & 1 \end{bmatrix}$$

$$\bar{A}_{dq1} =$$

$$\begin{bmatrix} 0.4321 & 0.0163 & 9.1123 & 0.3437 & -9.1123 & -0.3437 & 0.2837 & 0.0070 \\ -0.0163 & 0.4321 & -0.3437 & 9.1123 & 0.3437 & -9.1123 & -0.0070 & 0.2837 \\ -0.0445 & -0.0017 & 0.7157 & 0.0270 & 0.2836 & 0.0107 & 0.0501 & 0.0009 \\ 0.0017 & -0.0445 & -0.0270 & 0.7157 & -0.0107 & 0.2836 & -0.0009 & 0.0501 \\ 0.0445 & 0.0017 & 0.2836 & 0.0107 & 0.7157 & 0.0270 & 0.0055 & 0.0002 \\ -0.0017 & 0.0445 & -0.0107 & 0.2836 & -0.0270 & 0.7157 & -0.0002 & 0.0055 \\ 0 & 0 & 0 & 0 & 0 & 0 & 1 & 0 \\ 0 & 0 & 0 & 0 & 0 & 0 & 0 & 1 \end{bmatrix}$$

$$B_{1dq1} =$$

$$\begin{bmatrix} 0 & 0 \\ 0 & 0 \\ 0 & 0 \\ 0 & 0 \\ 0 & 0 \\ 0 & 0 \\ 0.0001 & 0 \\ 0 & 0.0001 \end{bmatrix}$$

$$K_{d1} =$$

$$\begin{bmatrix} -1218.41 & -62.37 & 6383.08 & 1232.97 & 23441.32 & 2106.23 & 5236.10 & 73.16 \\ 62.37 & -1218.41 & -1232.97 & 6383.08 & -2106.23 & 23441.32 & -73.16 & 5236.10 \end{bmatrix}$$

$$K_v v_1 =$$

$$\begin{bmatrix} 117.3282 & 11.5299 \\ 11.5299 & -117.3282 \end{bmatrix}$$

$$[P_{v1} \quad Q_{v1}]^T =$$

$$\begin{bmatrix} -5746.130 \\ -549.409 \end{bmatrix}$$

Grid Voltage	V	$120VRMS$
DC bus Voltage	Vdc	$350V$
Grid Frequency	$f\ (\omega c)$	$60Hz$ (376.99 rad/s)
Output Inductance	$Lo1$, $Lo2$, $Lo3$	$1.8mH$,$1.8mH$,$3.6mH$
Input Inductance	$Li1$, $Li2$, $Li3$	$1.8mH$,$5.4mH$,$3.6mH$
Filter Capacitance	$C1$,$C2$,$C3$	$8.8\mu F$
PWM Frequency	$fPWM$	$10kHz$
Sampling Period	Ts	$100\mu s$
[6[6Load 1	$R1$,$L1$	85.7Ω,$0.46H$
[Load 2	$R1$,$L1$	171.43Ω,$0.53H$
Error Weighting Matrix	$Qp1$,$Qp2$,$Qp3$	$\{5,4.9,4.8\}\times 103\times I2\times 2$
Input Weighting Matrix	$Rp1$,$Rp2$,$Rp3$	$\{0.2,0.15,0.18\}\times I2\times 2$
Inner Integrator Gain	$Ki1$,$Ki2$,$Ki3$	1
Outer Integrator Gain	$Ks1$,$Ks2$,$Ks3$	5
SOGI gain	KSG	0.7
PLL Proportional Gain	KpP	0.28307
PLL Integral Gain	KiP	7.5102
Frequency Restoration Gain	Kf	100
Power Rating	$S1$,$S2$,$S3$	500,1000,1500 VA
Voltage Restoration Gain (Active)	$Kp1$,$Kp2$,$Kp3$	1000,2000,3000
Voltage Restoration Gain (Reactive)	$Kq1$,$Kq2$,$Kq3$	−1000,−2000,−3000

9.2 Parameter Specifications

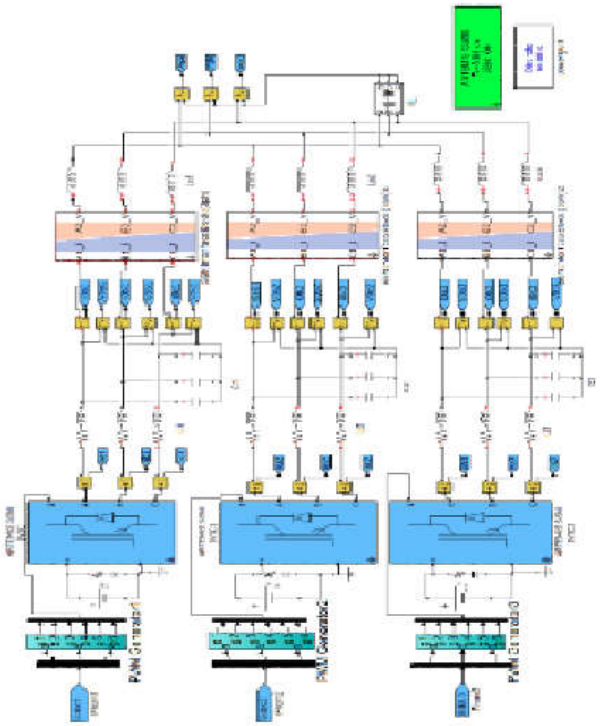

Fig No.9 State-vector mathematical model and the circuit in islanded mode in the ABC frame. TOP: Inverter 1. MID-DLE: Inverter 2 BOTTOM: Inverter 3

10. SMART LOAD (SL) Modelling and Interaction with Microgrid

To analyze such interactions and evaluate the performance, SS is developed for each of these following submodels and the respective state and input/output variables are defined. Finally, component Connection Method (CCM) [8][9] has been applied to obtain the overall SS of the model. Following subsections present the detail modelling of the linearized SS of smart Load SL. To reduce the number of dynamic equations and keep the analysis simple, the NCL (Non critical Load) has been considered to be of resistive type in this case. However, the analysis can be extended to any power factor of the NCL. Further, this model is extended to multiple smart load in a distribution feeder) and studies have been done to assess any unwanted interaction among the smart load (SL) and the network. The present scenario has been considered for 2 NCL Loads where Point of Load Voltage control (PoL) is applied for

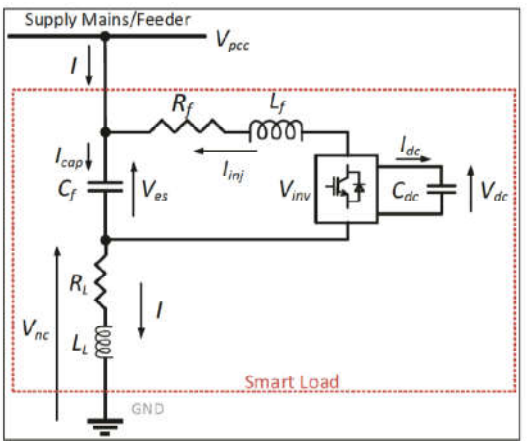

Fig No 10: SMART Load Schematic

Lf = Inductance of the SLQ converter

Rf = Resistance of the SLQ converter

Cdc= DC Link Capacitor

Idc= Dc current drawn by the DC Link capacitor

Vdc= Voltage across the DC link Capacitor

R_L,L_L= Resistance and Inductance of the Load

Vnc= Voltage across Non Critical Load

I= Current drawn by the Load

V_{es}= Voltage Compensation

Describing Equations:

$$Lf\frac{dIinj(t)}{dt} = Vinv(t) - Ves(t) - RfIinj(t)$$

$$Cf\frac{dVes(t)}{dt} = I(t) + Iinj(t)$$

(8)

$$Ll\frac{dI(t)}{dt} = Vpcc(t) - Ves(t) - Rl\,I(t)$$

$$Cdc\frac{dVdc}{dt} = Idc$$

10.1 PLL Models

The lead-lag compensator based single phase PLL implemented in Simulink is presented in Fig 11[14][15]. The PLL has one state variable corresponding to the lead-lag transfer function, denoted by α1 and α2 and a second one corresponding to the integrator, denoted by 1/s. The input and output variables considered for this sub-model are Vesq and θ . The typical value gain and time constant parameters are taken M = 2 and α1 = 0:001242, α2 = 0:02315.

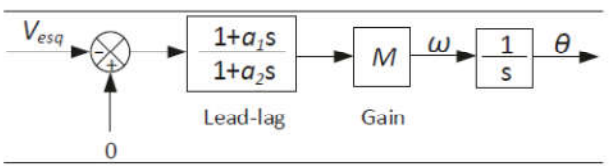

Fig 11: Simulink Model of Lead Lag Compensator based PLL

State space Model of PLL is represented by:

$$\begin{pmatrix}\Delta\omega\\ \Delta\theta\end{pmatrix} = \begin{pmatrix}M & 1-\frac{\alpha 1}{\alpha 2}\\ 0 & 0\end{pmatrix}\begin{pmatrix}0\\ 1\end{pmatrix}\begin{pmatrix}\Delta x1\\ \Delta\theta\end{pmatrix} + \begin{pmatrix}M\alpha 1/\alpha 2\\ 0\end{pmatrix}(\Delta Vesq) \quad (9)$$

10.2 Voltage Control Loops

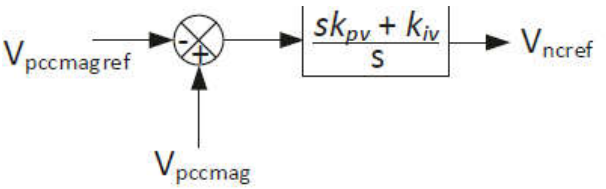

(a)

Fig No:12 (a) Schematic of PLL

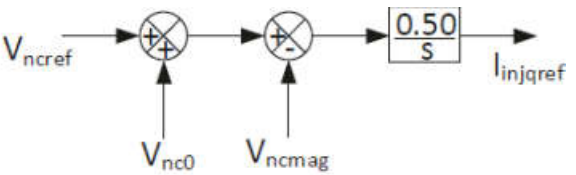

(b)

Fig No.12 (b) Schematic of NCL Loop control

$$(\Delta X21) = (\Delta X21)0 +$$

$$\begin{pmatrix}\frac{Vpccd0}{Vpccmag0} & \frac{Vpccq0}{Vpccmag0}\end{pmatrix}\begin{pmatrix}\Delta Vpccd\\ \Delta Vpccq\end{pmatrix} \quad (10)$$

$$(\Delta Vncref) =$$

$$(Kiv)\ (\Delta X21) +$$

$$\left(\left(\frac{Vpccd0}{Vpccmag0} \quad \frac{Vpccq0}{Vpccmag0}\right)\begin{pmatrix}\Delta Vpccd\\ \Delta Vpccq\end{pmatrix}\right) \quad (11)$$

10.3 Current Control Loop

The current control loop is identical for both the axes and the control loop architecture follows the standard design as used in any converter. Fig.13 presents the schematic diagram of the control loop[17][18]. The state variables for the d and q axis PI controllers are denoted by γd and γq, respectively and the controller gain parameters are given by *kpc* and *kic*. The small signal SS model of the current controller is given by.

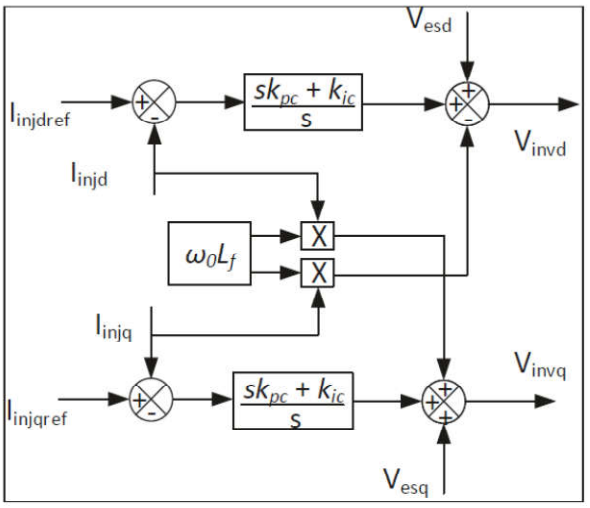

Fig No. 13 Current Control loop

$$\begin{pmatrix}\Delta Vinvd\\ \Delta Vinvq\end{pmatrix} = \begin{pmatrix}kic & 0\\ 0 & kic\end{pmatrix}\begin{pmatrix}\Delta Yd\\ \Delta Yq\end{pmatrix}\begin{pmatrix}Kpc & 0 & -kpc & -\omega 0\,Lf & 1 & 0\\ 0 & Kpc & \omega 0Lf & -kpc & 0 & 1\end{pmatrix} \quad (12)$$

$$\begin{bmatrix}\dot{\Delta\gamma d}\\ \dot{\Delta\gamma q}\end{bmatrix} = \begin{bmatrix}0 & 0\\ 0 & 0\end{bmatrix}\begin{bmatrix}\Delta\gamma d\\ \Delta\gamma q\end{bmatrix} + \begin{bmatrix}1 & 0 & -1 & 0 & 0 & 0\\ 0 & 1 & 0 & -1 & 0 & 0\end{bmatrix}\begin{bmatrix}\Delta I\ injdref\\ \Delta I\ injqref\\ \Delta I\ injd\\ \Delta I\ injq\\ \Delta Vesd\\ \Delta Vesq\end{bmatrix} \quad (13)$$

11. Control Methodology of Smart Load

Substantial proportion of industrial and service sector loads are induction motors.Motors which are directly connected to the supply inherently provide inertial response to the system unlike the drive-controlled motors which are decoupled from the supply[24][25]. Adjustable speed drives (ASD) are used to control the speed of the motor for improved performance and better energy utilization. With subtle modification to the ASD,it is possible to use the existing motor drives to control the power consumption of the motors over a short-time and thereby, contribute to rapid frequency response when needed. The proposed modification includes a frequency derivative loop to provide inertial response within the ramp rate limits An additional frequency support block is introduced along with the standard drive control. The measured deviation in grid frequency and RoCoF is used to modify the supply frequency reference for the motor. The rate of change of the motor frequency reference in response to the measured grid frequency variation has to be limited to avoid excessive regeneration especially, for drives with passive front-end. The above mentioned control scheme will enable a MSL(Motor Smart Load) to contribute to rapid frequency response by changing the

active power consumption of the motor according to the measured grid frequency and RoCoF. A drive controlled motor operating at a certain frequency (e.g. 45 Hz) would respond to an under-frequency event by reducing its operating frequency (e.g. down to 30 Hz) for a few seconds. For over frequency events, the motors would enter the constant-power mode beyond 50 Hz as V/f ratio is no longer maintained [23]. In such cases, the frequency support loop is disabled and the motor operates with standard drive control.

11.1 SLQ Capability (Smart Load Reactive Power Control Capability)

Capability plot for SLQ can be drawn in three simple steps using the previously Introduced SL equations. The first step involves calculating all possible values of V_{NC} using by sweeping the compensator voltage magnitude (V_{ES}) over a range of Values (0 to 1 p.u.) for two sets of phase angles (θ_{ES} = +90 and θ_{ES} =- 90).[10] This provides an exhaustive set of real positive values which can appear across NCL under different network disturbances. The second step includes calculating the smart load active and reactive power consumptions using the corresponding values of V_{NC} [8][11]. For SLQ type smart load P_{ES} should be considered zero in. The positive and negative sign of Q_{ES} signifies inductive and capacitive modes of the compensator. The positive value of P_{SL} corresponds to over-frequency disturbance. Q_{SL}>0 (Q_{SL}<0) represents increase (decrease) in smart load reactive power consumption for a certain change in P_{SL}.[9][12]

12 Simulation Results

To obtain simulation results, the circuit shown in Fig No 9 was implemented in MATLAB/Simulink using OPAL-RT ARTEMIS libraries. Main grid frequency and amplitude were selected to have nominal values. Fig. 62 shows the simulated output power of each inverter, the RMS voltage on the AC bus, and the microgrid frequency under different intervals of time.

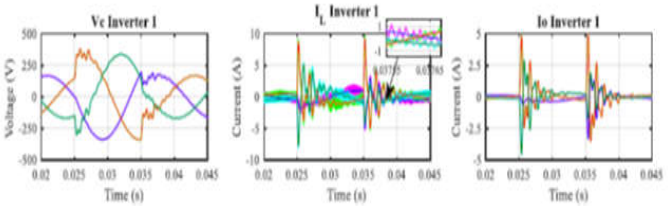

Fig No.14 (a) State-vector waveforms for the mathematical model and the circuit in islanded mode in the ABC frame. TOP: Inverter 1

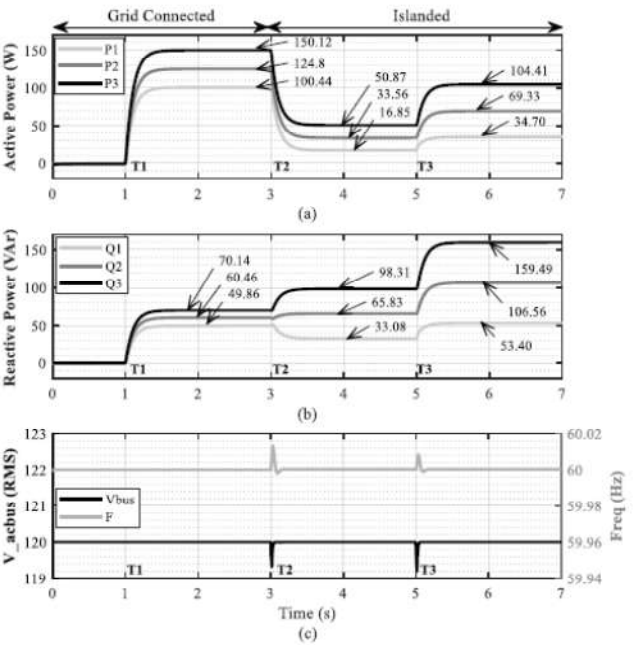

Fig No. 14(b) Simulation results. (a) Active power. (b) Reactive Power. (c) Voltage in the AC bus and frequency of the microgrid

12.1 Simulation Result Analysis

Analyzing Simulation result in Fig No. 14 (a) & (b) At $T1=1s$, an active power reference of 100W, 125W, and 150W was set for Inverters 1, 2, and 3 respectively. It can be seen that the three inverters have a damped response with a settling time of about 0.4 s and a steady-state error less than 0.2%.

At $T2=3$ s, the main grid is disconnected and the microgrid starts working in islanded mode with pair of smart load SL-1 connected. At this time, voltage and frequency on the AC bus are recovered in 0.05 s and 0.1 s, respectively. Active and reactive powers reach steady-state in 0.5 s and 0.3 s respectively. Also, generated power is proportionally shared between the three inverters according to their rated power capacity since ($P2/P1$ =33.5616.85 =1.991) ($P3/P1$=50.8716.85=3.018) ($Q2/Q1$=65.8333.08=1.990) (3/$Q1$=98.3133.08=2.971)

Finally, at $T3=5s$, Smart Load (SL-2)is connected. The voltage in the AC bus and the microgrid frequency show a disturbance of about 0.8 V and 0.01 Hz, respectively, with a recovery time of about 0.05 s and 0.1 s, zrespectively. In addition, active and reactive power have a settling time of about 0.3 s. Finally, active and reactive power remain proportionally shared between the three inverters since ($P2/P1$=69.3334.70=1.997) ($P3/P1$=104.4134.70=3.008)

($Q2/Q1$=106.5653.40=1.994)

($Q3/Q1$=159.4953.40=2.986) Simulation results confirm the effectiveness of the proposed controller in a computational environment.

13 Experimental Result Analysis:

Experimental results are presented islanded modes with smart Load connected for effective control of Microgrid. A complete Laboratory setup of Microgrid is created as shown in fig no15. For both modes, simulated and experimental results were obtained. For islanded mode, all inverters work as grid forming generators with frequency and amplitude close to nominal values. Also, active and reactive power demanded by the load are divided between generators according to their rated power value.

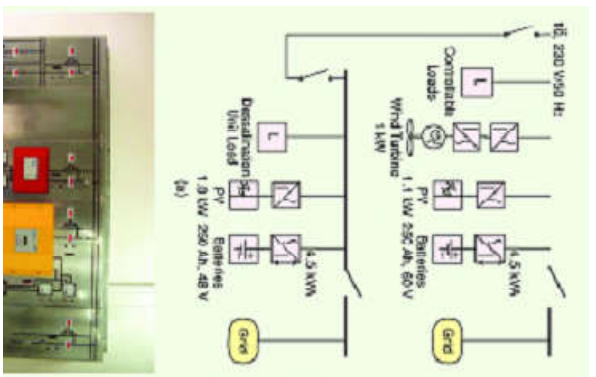

Fig No.15 Experimental Set up of Microgrid with Smart Load System

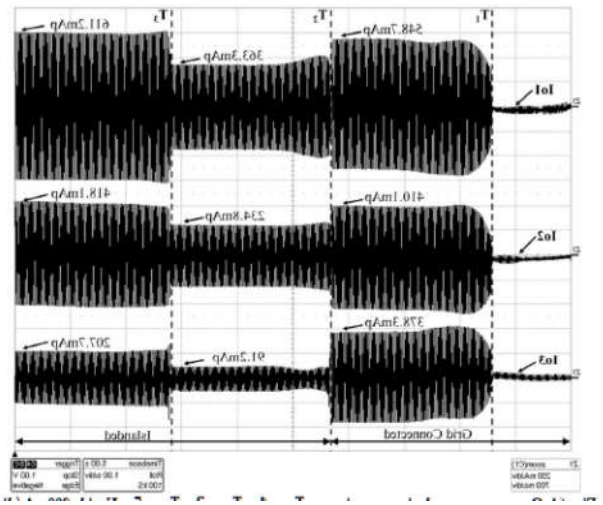

Fig No 16 Output currents during experiment. $T1$=1s, $T2$=3s, $T3$=5s. Vgrid=200mA/div, Hgrid=700ms/div

At $T1$=1s, an active power reference of 100W, 125W, and 150W was set for Inverters 1, 2, and 3, respectively based on availability of reserve power from PoL controller of smart load. Also, a reactive power reference of 50VAr, 60VAr, and 70VAr was set for Inverters 1, 2, and 3, respectively. It can be seen that the power shown in Fig. 14(b) and output currents shown in Fig. 16 for the three inverters have a damped response with a settling time of about 0.4 s and a steady-state error less than 0.3%.

At $T2$=3 s, the main grid is disconnected and the microgrid starts working in islanded mode with Load 1 connected. This means that the inverters work together as grid forming generators to deliver the power demanded by Load 1 and to recover voltage and frequency without communications. At this time, voltage and frequency on the AC bus are recovered in 0.8 s and 0.2 s, respectively. Active and reactive powers reach steady-state in 0.8 s and 0.5 s, respectively.

Finally, at $T3$=5s, Load 2 is connected. Voltage in the AC bus and frequency show a disturbance of less than 0.1 V and 0.01 Hz respectively with a recovery time of less than 0.3 s. In addition, active and reactive power have a settling time of about 0.4 s. Finally, active and reactive power remain proportionally shared between the three inverters

Conclusion: This work proposed a novel model and controller that integrate V-I and power sharing with smart load dynamics in a single state-space model. The model can be scaled to be implemented in islanded modes. For islanded mode, a mathematical procedure was developed to integrate any number of generators and loads in a single open-loop model that may be used for modern robustness. The proposed TCT controller for islanded and grid-connected microgrids improves transient response, accuracy on power sharing, and voltage and frequency restoration. It is worth to mention that the frequency and voltage restorations are performed without communications, which ensures robustness on the microgrid against abnormal conditions. Future work may

lead to investigating marginal stability of the unified microgrid-smart load by classical methods

References

[1] E. Rokrok and M. E. H. Golshan: 2010, "Adaptive voltage droop scheme for voltage source converters in an islanded multibus microgrid," *IET Gener. Transm. Distrib.*, vol. 4, no. 5, p. 562, 2010.

[2] U. Borup, F. Blaabjerg, and P. N. Enjeti, "Sharing of nonlinear load in parallel-connected three-phase converters," *IEEE Trans. Ind. Appl.*, vol. 37, no. 6, pp. 1817–1823, 2001

[3] Juan F. Patarroyo-Montenegro 1,*, Jesus D. Vasquez-Plaza 1, Fabio Andrade 1 and Lingling Fan 2An Optimal Power Control Strategy for Grid- Following Inverters in a Synchronous Frame" Applied Science 2020 ,10 ; doi:10.3390/app10196730

[4] J. C. Vasquez, J. M. Guerrero, M. Savaghebi, J. Eloy-Garcia, and R. Teodorescu, "Modeling, analysis, and design of stationary-reference-frame droop-controlled parallel three-phase voltage source inverters," *IEEE Trans. Ind. Electron.*, vol. 60, no. 4, pp. 1271–1280, 2013.

[5] Juan F. Patarroyo-Montenegro *, Jesus D. Vasquez-Plaza and Fabio Andrade "A State-Space Model of an Inverter-Based Microgrid for Multivariable Feedback Control Analysis and Design" Energies 2020, 13, 3279; doi:10.3390/en13123279

[6] Q. Shafiee, J. M. Guerrero, and J. C. Vasquez, "Distributed Secondary Control for Islanded MicroGrids - A Novel Approach," *IEEE Trans. Power Electr.*, vol. 29, no. 2, pp. 1018–1031, 2014.

[7] A. R. Bergen and V. Vittal, "Power Systems Analaysis," *Department of Electrical Engineering*. pp. 103–127, 2007.

[8] Diptargha Chakravorty, Jinrui Guo, Balarko Chaudhuri, Ron Hui" Small Signal Stability Analysis of Distribution Networks with Electric Springs" *IEEE Trans. Smart Grid.*, vol. 10, no. 2, pp. 1533–1552, 2019

[9]Diptargha Chakravorty, Balarko Chaudhuri, Shu Yuen Ron Hui" Estimation of Aggregate Reserve with Point-of-Load Voltage Control" *IEEE Trans. Smart Grid.*, vol. 9, no. 5, pp. 4649–4658, 2018

[10]E. A. A. Coelho, P. C. Cortizo, and P. F. D. Garcia, "Small-signal stability for parallel-connected inverters in stand-alone ac supply systems," *IEEE Trans. Ind. Appl.*, vol. 38, no. 2, pp. 533–542, 2002.

[11] M. Hao and X. Zhen, "A control strategy for voltage source inverter adapted to multi - Mode operation in microgrid," *Chinese Control Conf. CCC*, pp. 9163–9168, 2017.

[12] J. Pou, "Modulation and Control of Three-Phase PWM Converters," Ph.D dissertation, Dept. Elect. Eng., Univ. Politècnica de Catalunya, Terrassa, Spain, 2002.

[13]F. L. Lewis, D. L. Vrabie, and V. L. Syrmos, *Optimal Control*. Hoboken, NJ, USA: John Wiley & Sons, Inc., 2012.

[14] J. F. Patarroyo-Montenegro, M. Castellà, F. Andrade, K. Kampouropoulos, L. Romeral, and J. Vasquez-Plaza, "An Optimal Tracking Power Sharing Controller for Inverter-Based Generators in Grid-connected Mode," in *IECON Proceedings (Industrial Electronics Conference)*, 2019.

[15] R. Teodorescu, M. Liserre, and P. Rodríguez, *Grid Converters for Photovoltaic and Wind Power Systems*. Chichester, UK: John Wiley & Sons, Ltd, 2011.

[16] dSPACE Systems, “Online catalog,” 2018. [Online]. Available: https://www.dspace.com/en/pub/home/medien/product_info/catalog_contents.cfm.

[17] C. E. Shannon, “Communication in the Presence of Noise,” *Proc. IRE*, vol. 37, no. 1, pp. 10–21, Jan. 1949

[18] Y.Wang, X.Wang, F. Blaabjerg, and Z. Chen, \Small-signal stability analysis of inverter-fed power systems using component connection method," IEEE Transactions on Smart Grid, vol. PP, no. 99, pp. 1{1, 2017.

[19] H. Allcott, \Real time pricing and electricity markets," 2009.

[20] A. Hughes and B. Drury, Electric Motors and Drives. Elsevier Ltd., 4th ed 2013.

[21] X. Luo, Z. Akhtar, C. K. Lee, B. Chaudhuri, S. C. Tan, and S. Y. R. Hui, \Distributed voltage control with electric springs: Comparison with STATCOM,"IEEE Transactions on Smart Grid, vol. 6, no. 1, pp. 209{219, 2014.

[22] Z. Akhtar, B. Chaudhuri, and S. Y. R. Hui, \Smart loads for voltage control in distribution networks," IEEE Transactions on Smart Grid, vol. 8, pp. 937{946, March 2017.

[23] Z. Akhtar, B. Chaudhuri, and R. Hui, \Primary Frequency Control Contribution from Smart Loads Using Reactive Compensation," IEEE Transactions on Smart Grid, vol. 6, no. 5, pp. 2356{2365, 2015.

[24] A. Tuladhar, H. Jin, T. Unger, and K. Mauch, “Parallel operation of single phase inverter modules with no control interconnections,” in *Proceedings of APEC 97 - Applied Power Electronics Conference*, 1997, vol. 1, pp. 94–100.

[25] Y. Shuo, S. C. Tan, C. K. Lee, and S. Y. R. Hui, \Electric spring for power quality improvement," in IEEE Applied Power Electronics Conference and Exposition (APEC), pp. 2140{2147, 2014.

[26] D. Chakravorty, B. Chaudhuri, and S. Y. R. Hui, \Rapid frequency response from smart loads in great britain power system," IEEE Transactions on Smart Grid, vol. PP, no. 99, pp. 1{1, 2016.

[27] S. Yang, Q. Lei, F. Z. Peng, and Z. Qian, “A robust control scheme for grid-connected voltage-source inverters,” *IEEE Trans. Ind. Electron.*, vol. 58, no. , pp. 202–212, 2011.

Aniruddha Bhattacharya (1976-) is Assistant Professor at Electrical Engineering Department of Delhi Technological University. He has received his BE and ME degrees at Pune University.

Madhusudan Singh (1963-) Professor at Electrical Engineering Department of Delhi Technological University